Current-Driven Dynamics in Molecular Junctions: Endohedral Fullerenes

Ryan Jorn,[†] Jin Zhao,[‡] Hrvoje Petek,[§] and Tamar Seideman[†,*]

[†]Department of Chemistry, Northwestern University, 2145 Sheridan Road, Evanston, Illinois 60208-3113, United States, [‡]Physics Department, Hefei National Laboratory for Physical Sciences at Microscale, University of Science and Technology of China, Hefei, Anhui, China, and [§]Department of Physics and Astronomy and Petersen Institute for NanoScience and Engineering, University of Pittsburgh, Pittsburgh, Pennsylvania 15260, United States

ABSTRACT We introduce a new paradigm for single molecule devices based on electronic actuation of the internal atom/cluster motion within a fullerene cage. By combining electronic structure calculations with dynamical simulations, we explore current-triggered dynamics in endohedrally doped fullerene molecular junctions. Inelastic electron tunneling through a Li atom localized resonance in the Au—Li@C_{60}—Au junction initiates fascinating, strongly coupled 2D dynamics, wherein the Li atom exhibits large amplitude oscillation with respect to the fullerene wall and the fullerene cage bounces between the gold electrodes, slightly perturbed by the embedded atom motion. Implications to the fields of single molecule electronics and nanoelectromechanical systems are discussed.

KEYWORDS: molecular electronics · fullerenes · metallofullerenes · current-induced dynamics · electron scattering · SAMO

Since the early days of their discovery, fullerenes have generated intense interest for both their fundamental properties and potential uses as chemical capsules.[1−4] Synthetic techniques have made it possible to entrap a variety of atoms and molecules inside the carbon cage of fullerenes, including nobel gases,[5,6] small molecules,[7−9] and metal atoms and clusters.[1,4] Efforts to perfect "molecular surgery" suggest that this list of guest species will only continue to grow.[2,9] As the number of endohedrally substituted atoms and molecules has increased, so have the variety of proposed applications for fullerene-based materials, ranging from medicinal, such as delivery of radiopharmaceuticals[10,11] and MRI contrast agents,[12,13] to hydrogen storage[7] and quantum computing.[14] In addition to the aforementioned avenues, the encapsulation of metals in fullerenes is of particular interest to the field of molecular electronics, where the adatoms and clusters may act as dopants or even active elements for enhanced conduction and conduction switching in molecule-based circuitry.[3,8,15,16] Conductance measurements have been performed on fullerenes and their derivatives in the context of both single molecules[17−22] and thin films.[23,24] Recent work[16,25−27] on the diffuse atom-like orbitals of C_{60} (denoted superatom molecular orbitals or SAMOs) highlights the potential of endoheral metallofullerenes to play a role in molecular electronics.

In addition to their conductance characteristics, fullerenes also demonstrate unique dynamics during current transmission,[18,19,28] which make them attractive candidates for molecular machines.[29,30] Although the concept of current-driven dynamics and its application to design new forms of molecular machines is very general,[29,30] the case of fullerene-based junctions offers several unique features, including simple, one-dimensional, atom-like motion and a variety of potential technological applications, as explored previously.[28,31] Endohedral fullerenes are particularly interesting as molecular machines because the actuation of the internal atom/cluster motion can change the electronic properties of the molecule without altering the molecular shape. The transient electron tunneling through SAMO resonances presents an opportunity for studying internal femtochemistry as a means of actuating single molecule devices. Recent theoretical and experimental research has explored a broad variety of current-driven phenomena in molecular junctions, ranging from small amplitude vibrations to complex molecular machines and bond breaking phenomena.[32]

The mechanism of current-driven dynamics in molecular-scale electronics is well understood.[30] Resonances are ubiquitous in molecular junctions and resonant transport is often inelastic. The tunneling event promotes the molecule transiently to a charged or partially charged resonance (an anion state corresponding to electron scattering, that is, conductance *via* an empty orbital or a cation state corresponding to hole scattering and conductance *via* an occupied orbital). Electronic relaxation is typically fast, but in general the initial and resonant states

* Address correspondence to t-seideman@northwestern.edu.

Received for review June 4, 2011 and accepted August 31, 2011.

Published online August 31, 2011
10.1021/nn202589p

are displaced in equilibrium and, hence, the system evolves along its nuclear coordinates during the resonance lifetime.This is true both for a fullerene molecule sandwiched by metal electrodes, as well as the species included within a fullerene cage. Upon electronic relaxation, the endohedral fullerene is internally excited and interesting dynamics are likely to ensue.

Our goal in the present study is to explore the inelastic electron driven nuclear dynamics of one of the simplest known endohedral fullerenes, Li@C_{60}. Our work builds on the previous theoretical studies of current-driven dynamics in fullerene junctions[28,31,33] by including both the center-of-mass and internal coordinate dynamics. We will take advantange of the lowest lying SAMO, the atom-like *s*-symmetry molecular orbital, in the current-induced dynamics of a Li@C_{60} molecule. Experimentally, this endohedrally doped fullerene has shown promise for enhanced conductance relative to C_{60}[24] as well as amplified optical properties.[34] Several authors have considered the electronic structure of Li inside fullerenes using Hartree–Fock[35] and various density functional theory (DFT) methods.[16,36–42] The results of these studies point to a significant charge transfer in the ground state of an isolated molecule between the Li and the fullerene cage, corresponding to at least +0.6e, dependent on the position of the atom inside the carbon shell.[37,40] As a result of the Coulomb interaction between the Li atom and the carbon cage, the atom is displaced from the center of C_{60} by approximately 1.5 Å. Doping C_{60} with metal atoms has also been shown to influence its SAMOs by reducing the LUMO–SAMO energy gap[16] through hybridization between *s*-symmetry states of the atom and the hollow cage. In the case of Li, this interaction reduces the LUMO–SAMO gap from 3.28 to 1.10 eV when the Li atom is at the center and to 2.05 eV when Li is in its ground state equilibrium position. This sensitivity of the *s*-SAMO to the position of the Li atom introduces coupling of the electron and nuclear motions, making Li@C_{60} an intriguing system for understanding the actuation of internal atom/cluster motions in endohedral fullerene based molecular machines.

Regarding the dynamics of Li inside the fullerene, investigations have been carried out both experimentally, using IR and Raman spectroscopies,[43] as well as theoretically by simulating rotational/vibrational spectra of isolated molecules.[44–46] The modeling efforts have largely relied on solving a three-dimensional Schroedinger equation for the Li atom subject to an interaction potential with a stationary carbon cage. While Li is often assumed in these studies to be held in a spherically symmetric potential well, recent work has suggested that this is an idealization and, in reality, the Li atom experiences the corrugation of the carbon shell with small barriers existing between the various hexagonal and pentagonal sites that localize the low-lying Li nuclear wave functions.[36,44]

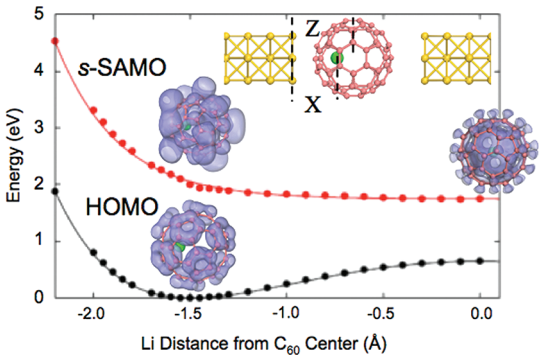

Figure 1. Potential energy curves for Li motion within the C_{60} along with iso-surface plots of the relevant orbitals and a schematic of the fullerene junction. Carbon atoms are indicated in orange and the Li atom in green. DFT energies (solid circles) and functional fits (curves) are shown for the potential energy along the coordinate for Li atom motion in the C_{60} for the ground (black) and the resonance (red) states. The HOMO of the Li@C_{60} and the *s*-SAMO are shown above the black and red curves respectively. On the left side of the graph, above the ground state potential well, both orbitals are depicted for Li at the ground state equilibrium position, whereas the s-SAMO for Li at the center of the C_{60} is shown on the right side. Finally, the model junction envisioned is depicted in the inset, where the two degrees of freedom studied are indicated by X, the Li motion, and Z, the center-of-mass translation coordinate of the C_{60}, both measured with respect to the center of the top layer of the gold atoms of the left electrode.

Here we introduce a new and fascinating field of research that ties together the transport and dynamical properties of endohedrally doped fullerenes discussed above which, in addition, carries interesting potential applications. Specifically, we envision a molecular electronic junction, where a Li adatom embedded in a fullerene cage is, in turn, contacted to two metallic electrodes and driven by a current excited between them. Our goal is to model the internal femtochemistry induced by the charge transmission through the Au–Li@C_{60}–Au junction and apply the results to understand the potential impact of doped fullerenes on the fields of molecular electronics and nanoelectromechanical systems (NEMS). In the following section, we describe the potential energy surface for the relevant nuclear degrees of freedom for current-induced motion in a Au–Li@C_{60}–Au junction, focusing on the dynamical properties conferred by the *s*-SAMO resonance and discuss the interplay between the Li and fullerene dynamics. In the final section, we conclude with several remarks on the impact of these results on the field of fullerene molecular junctions and on avenues for future theoretical and experimental research.

ELECTRONIC STRUCTURE

The dynamics of the Li atom within the C_{60} cage were based on potential energy curves calculated by density functional theory (DFT). The resulting HOMO and *s*-SAMO are shown on the left-hand side of Figure 1 with the Li atom at its equilibrium position, centered on

TABLE 1. Potential Energy Fitting Parameters for eq 1, with Distances in Å and Energies in eV

parameter	value
$D_{C_{60}}$	1.0000
$\alpha_{C_{60}}$	0.9677
V_N^0	2.9900
D_{Li}	1.8379
α_{Li}	1.0374
X_{eq}	1.5349
Δ_{eq}	0.1600
V_E^0	2.7250
F_0	2.8106×10^{-2}
β	3.1356

a hexagonal face of the fullerene. Comparison of the HOMO of Li@C_{60} in Figure 1, with that of a bare C_{60} molecule (not shown) indicates that the asymmetric position of the Li atom within the fullerene cage hardly perturbs the HOMO distribution, because the constituent C 2p orbitals are strongly bound to C atom cores. This is in fact true for all of the σ and π orbitals of fullerenes. In contrast, as noted in previous work, the asymmetric location of the Li atom perturbs the spherical symmetry of the SAMO, but the high degree of delocalization of the orbital is still retained. The sensitivity of the SAMO to the position of the Li atom derives from hybridization with the 2s orbital of Li, and is evident in Figure 1, which compares the *s*-SAMO with the Li placed at its equilibrium positions in the ground (left-hand side) and the excited state (right-hand side). One can expect strong coupling to be induced between the electron and Li atom motions by transient electron scattering through the *s*-SAMO resonance, which projects a ground state wave packet onto the *s*-SAMO surface far from its equilibrium position.

Dunlap et al.[42] similarly investigated the ground state $M^+@C_{60}^-$, where M stands for an alkali atom, and the excited charge-transfer state of M@C_{60} using local basis sets and the ΔSCF method. Their excited potential energy curve likewise has a minimum at the center of the cage. One can see from the potential energy curves for the system in Figure 1 that the equilibrium position of the Li atom in the ground state is about 1.5 Å displaced from the center of the C_{60} and the depth of the well, created predominantly by the Coulomb interaction with the carbon cage, is about 0.65 eV. Our results for the equilibrium position, well depth, and vibrational frequency, 353 cm^{-1}, are in good agreement with previous calculations.[36,38,40,42,45,46]

We consider a molecular junction whose general construction is shown in the inset of Figure 1. The metallic electrodes break the spherical symmetry of the Li nuclear wave function and restrict the motion of the atom to one dimension, namely, the coordinate along which current drives the system (the *X*-coordinate in Figure 1). Following previous work, the dispersion interaction between the fullerene and the gold electrodes is accounted for by using a Morse potential

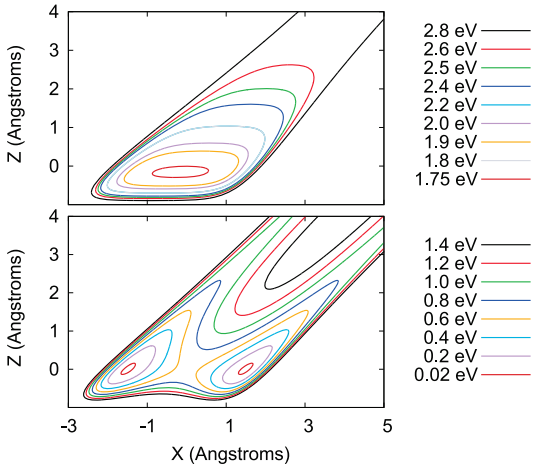

Figure 2. Potential energy surfaces, see eq 1, for the initial (lower panel) and the resonance (upper panel) states.

for the center-of-mass coordinate, *Z*.[33] Studies of the charged states of Li@C_{60} indicate that the charge distribution is not greatly effected by the adatom,[39] allowing us to make use of the shifted potential model first suggested in ref 17. Within this model, the additional charge is assumed to be distributed across the carbon shell and interacts with its image in the metal electrode. The image charge interaction shifts the equilibrium of the C_{60} center-of-mass closer to the electrode surface, resulting in a charged state potential curve, which is shifted in equilibrium with respect to the ground state but is not altered in shape. At relevant interelectrode distances, the C_{60} is in chemical contact with only one of the two electrodes and the second electrode does not directly modify the nuclear dynamics. It effects the electronic dynamics, however, *via* its influence on the resonance lifetime. The functional form of the two-dimensional potential surface in terms of the coordinates of Figure 1 is given by

$$\begin{aligned} V_N &= D_{C_{60}}(e^{-2\alpha_{C_{60}}Z} - 2e^{-\alpha_{C_{60}}Z}) \\ &\quad + D_{Li}(e^{2\alpha_{Li}(X - Z - X_{eq})} - 2e^{\alpha_{Li}(X - Z - X_{eq})}) \\ &\quad + D_{Li}(e^{-2\alpha_{Li}(X - Z + X_{eq})} - 2e^{-\alpha_{Li}(X - Z + X_{eq})}) + V_N^0 \\ V_E &= D_{C_{60}}(e^{-2\alpha_{C_{60}}(Z + \Delta_{eq})} - 2e^{-\alpha_{C_{60}}(Z + \Delta_{eq})}) \\ &\quad + F_0(e^{\beta(X - Z)} + e^{-\beta(X - Z)}) + V_E^0 \end{aligned} \quad (1)$$

where V_N is the initial state potential and V_E corresponds to the resonance state. The various parameters are defined in Table 1 and the resulting two-dimensional surfaces are plotted in Figure 2. It should be noted that the actual well depth and the equilibrium distance differ from the standard interpretation of the Morse potential parameters as a result of the overlapping ranges between the two functions that constitute the 2D (center-of-mass and Li atom motion) surfaces.

CURRENT-DRIVEN DYNAMICS

Figure 3 illustrates the nuclear dynamics resulting from the instantaneous promotion of the nuclear wave

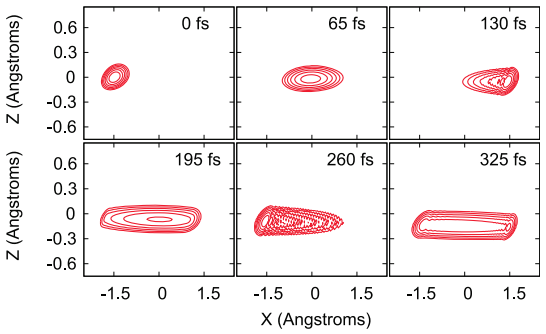

Figure 3. Snapshots of the probability density in the resonance state as a function of time. The contours correspond to probability densities from 10^{-8} to 10^{-3} and the time at each snapshot is indicated in the respective panel.

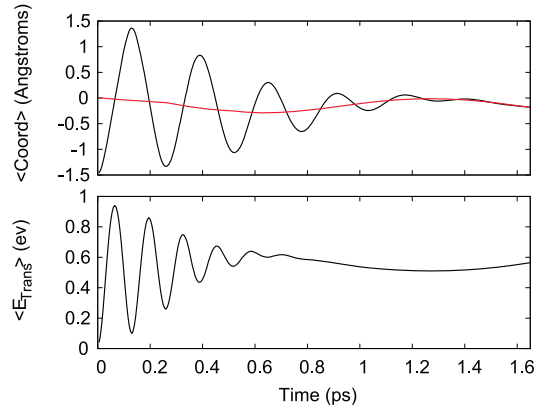

Figure 4. Expectation values of the *X*- and *Z*-coordinates (a) and of the energy transferred to the nuclear system as a result of electron scattering (b). In (a), $\langle X \rangle$ is given by the black curve and $\langle Z \rangle$ by the red curve.

function onto the excited anion state during the electron scattering event. As is clear from the first 325 fs of the evolution, the Li atom initially finds itself on a repulsive wall of the resonance surface, which kicks it toward the center of the fullerene cage. After 130 fs, the wave packet encounters the far wall of the fullerene and is reflected back toward its starting position. Subsequent dynamics involve the continued oscillation of the Li atom between the two walls of the fullerene cage, as shown in Figure 4, which is accompanied by wave packet dephasing as a result of the anharmonicity of the resonance potential. The dephasing expresses itself, Figure 3, by the spreading of the wave packet in the *X*-coordinate and the gradual decay of the oscillation amplitude of $\langle X \rangle$ (see Figure 4). Motion in the *Z*-coordinate in the resonance state is much smaller in amplitude, because the extent of the dynamics is determined by the shift in equilibrium position, Δ_{eq}, between the two potential energy surfaces. Given that Δ_{eq} is on the order of tens of picometers, the resulting oscillation amplitude is an order of magnitude smaller than that of the lithium dynamics, as evidenced by Figure 4. The period of motion in the center-of-mass coordinate is nearly 2 orders of magnitude

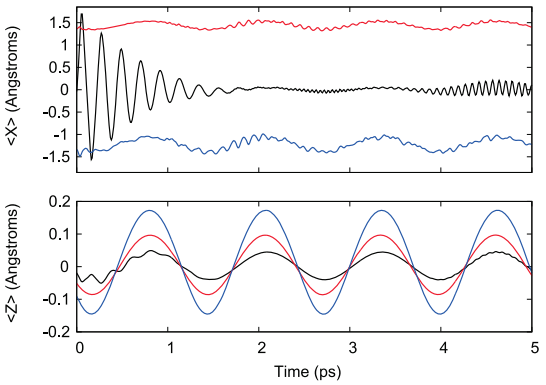

Figure 5. Expectation values of the *X*- and *Z*-coordinates upon relaxation to the neutral state after residence times of 65 fs (black), 130 fs (red), and 260 fs (blue) .

larger than that for the induced lithium oscillations, which implies that the center-of-mass motion will not be heavily influenced by the details of the rapid lithium dynamics. Rather, the fullerene will experience only an effective interaction averaged over multiple lithium vibrational periods and, given the symmetry of the potential about $X = 0$, one might expect this averaged interaction to be small. From a purely classical standpoint, one would intuitively expect that, due to the large mass disparity between the fullerene and the Li, the impulse imparted by the Li motion will not greatly effect the fullerene motion. Calculation of the energy transferred to the nuclei as a function of the residence time substantiates the above qualitative anticipation, see Figure 4. Maxima in the energy transferred occur at half the period of the $\langle X \rangle$ oscillations. These maxima in energy correspond to residence times in the resonance state where the atom has acquired substantial kinetic energy and is projected onto high energy portions of the ground state potential, both conditions being fulfilled at $X = 0$.

Upon relaxation to the neutral state, the induced dynamics follow the oscillations of the Li atom and the fullerene on the resonance surface. For residence times when the Li atom is at *X*-values corresponding to the barrier region of the ground state, that is, maxima in the energy transferred (see Figure 4), a large portion of the wave packet is projected onto eigenstates above the barrier and the largest amplitude neutral state motions are observed. This is evident in Figure 5, where the *X*-motion following the relaxation to the neutral state after a residence time of $\tau_R = 65$ fs shows the Li atom shuttling between the two minima of the potential. As the Li atom approaches *X* regions in the resonance state that correspond to the well regions of the ground state, the dynamics upon relaxation to the neutral state become more confined and the Li atom is again trapped in a local minimum. Hence, for residence times of 130 and 260 fs, the atom remains localized within one of the double-well minima in the ground state. It is of interest to note that even in these circumstances, the system experiences some additional

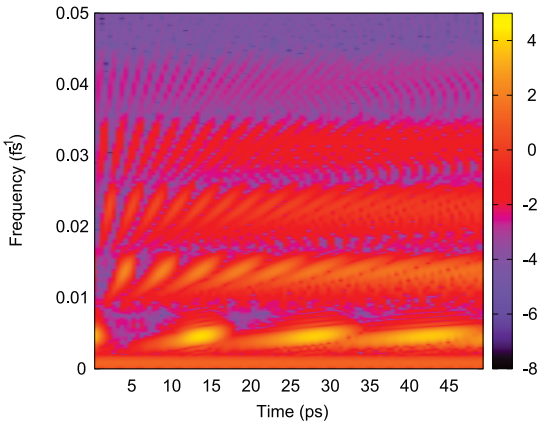

Figure 6. Logarithm of the time-windowed power spectrum for the expectation value of *X* for the first 50 ps in the neutral state subsequent to a residence time of τ_R = 65 fs. The first five picoseconds of the evolution of $\langle X(t)\rangle$ are shown in Figure 5. The power is plotted on a logarithmic scale and the details of the windowing procedure are discussed in the text.

oscillation in the lithium coordinate, however, at the frequency of the center-of-mass motion rather than at that of the purely lithium vibration. These oscillations correspond to nonadiabatic coupling between the fullerene and Li vibrations, that is, the fullerene moving sufficiently fast to perturb the eigenstates in the *X*-coordinate. The effect of the lithium motion on the C_{60} coordinate are negligible for τ_R corresponding to trapping the atom in the minima of the ground state, which is in accord with our intuitive anticipations sketched above. Surprisingly, however, signatures of the lithium oscillation at instances when the energy transferred to the *X*-coordinate is at a maximum can be recognized. Thus, the lithium motion is able to induce excitation of the fullerene dynamics, despite the large mismatch in masses.

The behavior of $\langle X(t)\rangle$, as shown in Figure 5, demonstrates the presence of multiple time scales in the wave packet dynamics. In particular, for a residence time of 65 fs, one sees the initial oscillation of the Li as it shuttles between the wells of the potential, followed by a second very low amplitude oscillation from 2 to 4 ps, which corresponds to the center-of-mass motion and, finally, a much higher frequency component that appears after 4 ps. While the former two frequencies have obvious physical origins, the puzzling presence of the high frequency component lead us to investigate time-windowed Fast Fourier Transforms of the $\langle X(t)\rangle$ signal. The window selected for the analysis was the $\cos^2(\pi(t - t_0)/T)$ function, also known as the Hanning window,[47] where the time origin (t_0) is varied to sample the signal and the width of the time-window (T) was taken as 300 fs. A plot of the logarithm of the resulting power spectrum is shown in Figure 6. One can clearly see a continuous band located along the bottom of the graph near zero frequency, corresponding to the fullerene oscillation. The next highest band, located around

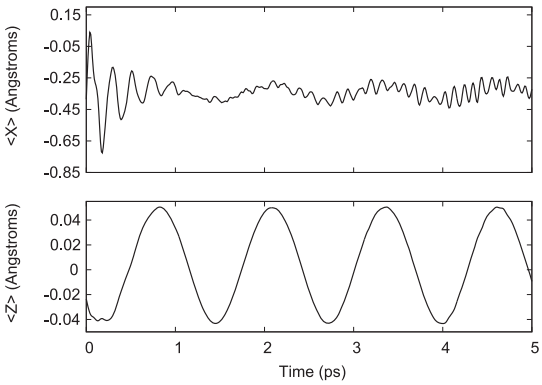

Figure 7. τ_R-averaged expectation values of the *X*- and *Z*-coordinates upon relaxation to the neutral state.

0.005 fs^{-1}, corresponds to the frequency of the initial Li bouncing motion, which undergoes continual dephasing and rephasing in the power spectrum in accordance with the revival time for the Li shuttling motion. One also observes regularly spaced structures at higher frequency, which grow and disappear in time in a similar fashion, but on shorter time scales. These structures correspond to fractional revivals of the system and explain the origin of the signature seen in $\langle X(t)\rangle$ for a 65 fs residence time (see Figure 5). Such fractional revivals have been studied previously in the context of vibrational and rotational wave packets for simple molecules[48] and form an intriguing avenue for future research.

The τ_R-averaged expectation values, shown in Figure 7, capture all of these rich quantum dynamics for both coordinates. In the *X*-degree of freedom, we see the lithium motion induced by the nonadiabatic electron transfer producing a shuttling motion between the ground state minima for the first picosecond. This is followed by oscillations in the lithium coordinate resulting from nonadiabatic coupling to the C_{60} motion. The τ_R-averaged center-of-mass dynamics, $\langle Z\rangle$, is impacted to only a minor extent by the nonadiabatic coupling to the Li atom vibration over the relevant time scales.

CONCLUDING REMARKS

Previous research has discussed the transport properties of endohedrally substituted fullerenes and their potential in molecular electronics. Above, we complemented this research with a prediction of the current-driven dynamics of substituted-fullerene-based junctions. Specifically, we addressed the case of Au−Li@C_{60}−Au conductance junctions subject to resonant current. We found fascinating coupled two-dimensional dynamics, wherein the C_{60} cage bounces against the gold electrode, slightly perturbed by the embedded atom, while the Li atom exhibits higher frequency, large amplitude oscillations with respect to the fullerene wall, which are strongly coupled to the C_{60} center-of-mass translation. Essential to these motions is an inelastic, resonant tunneling event involving a partially charged state of the Li@C_{60} system.

Our present work invites several interesting avenues for future research on current-driven dynamics in endohedral-fullerene-based junctions. As discussed above, our present theory does not take into account dissipation due to coupling with the electrode phonons and electron–hole pairs. An interesting challenge for future theoretical work would thus be an application of the ensemble scattering formalism of ref 32. to the problem at hand. Furthermore, the nonradiative coupling between the *s*-SAMO and the underlying HOMO and LUMO states, particularly in the presence of the large amplitude internal motion deserves further study.

Although the phenomenon of current-driven dynamics in molecular-scale electronics is very general, the example of substituted-fullerene-based junctions emerges as a specifically interesting case. In particular, it offers large amplitude yet stable motion, of potential application for nanoelectromechanical systems, along with widely tunable properties, adjusted by choice of the dopant and the fullerene size and the dopant ionization potential. Here we described the simplest case of atom shuttling (translation) within a fullerene cage, but we envision more complex motions, such as endohedral cluster rotations and vibrations, to provide additional dynamical degrees-of-freedom for modulating electron tunneling within metal-endohedral fullerene-metal junctions. Moreover, the encapsulation of magnetic atoms or clusters in a fullerene cage would offer spin dynamics to be coupled with the internal and center-of-mass motions.

Finally, an experimental realization of our predictions would be exciting. Evidence for excitation of the internal, as well as the center-of-mass motions, could be potentially gleaned through frequency domain STM measurements, such as the inelastic electron tunneling or the action spectroscopy.[19,49] A far more exciting prospect is to actuate and observe the endohedral fullerene rattling motion directly in the time domain by coupling femtosecond laser pulses into an STM tunneling junction. As in the case of alkali atoms on noble metals,[50] excitation of a charge-transfer transition by light can transiently occupy *s*-SAMO to initiate the internal femtochemistry. Although STM electronics are too slow to follow the ensuing nuclear wave packet motion, the coherent THz polarization associated with the nuclear dynamics could be detected with extreme sensitivity in pump-probe experiement at kHz frequencies by detecting the modulation of STM current, as is commonly done in the case of coherent phonon spectroscopy.[51] One advantage of employing the translationally one-dimensional rattling motion of endohedral fullerenes for ultrafast STM measurements with respect to other embodiments of single molecule switches, for example, based on conformational isomerization, is that the junction can be actuated continuously with the endohedral fullerene maintaing a constant outward shape while the internal atom/cluster motion modulates the junction conductivity. Such experiments are currently under way in our laboratories.

METHODS

Single point energy calculations were carried out within density functional theory and fitted to functional forms to generate potential curves for the Li motion in the *s*-SAMO derived and the ground (HOMO) states. The generalized gradient approximation was coupled with the PBE functional in the Vienna *ab initio* simulation package (VASP) using a plane wave basis set. The cubic unit cell with dimension of 3.0 nm contained a single C_{60} molecule. The projector augmented wave (PAW) method was used to describe the electron–ion interaction and the plane wave basis set cut off energy was set to 400 eV. The potential energy curves for the Li atom motion inside the fullerene cage were calculated by varying its position along the line passing from the C_{60} molecule center through the center of a hexagonal face in both the ground and the *s*-SAMO derived anion state $Li@C_{60}^-$. A Koopman-type approximation was made to calculate the excited electronic potential energy curve for the anion when the *s*-SAMO is occupied. By adding the Kohn–Sham energy of the SAMO to the ground state values, we obtained an approximation to the potential curve for the excited resonance surface.

As noted by previous authors, the shape of the ground state is well approximated by a Morse potential and this observation was used in our model to simplify the interaction potential. A Morse function for modeling the nuclear dynamics was obtained by a nonlinear least-squares fit of the *ab initio* data. The approximate excited state is not as smooth as the ground state curve, but can be fit accurately to an exponential function. The *ab initio* data and the nonlinear fits are shown in Figure 1. (Only half of the Li coordinate range is shown in Figure 1 because the potential curves are symmetric with respect to the center of the C_{60}.)

As mentioned at the outset, an accurate description of the resonance scattering dynamics requires a proper account of the nonequilibrium physics, the open boundary in the electronic subspace, and the coupling of the nuclear dynamics to phonons and electron–hole pair excitations in the two electrodes. These events, along with the strongly nonadiabatic vibronic dynamics, are captured within the density matrix scattering formalism of ref 32; see also ref 28. In the present study a much more qualitative model is invoked, which was originally put forth by Menzel and Gomer,[52] as well as Redhead,[53] to describe desorption induced by electron scattering off adsorbates on metal surfaces and was later extended and applied to surface femtochemistry in the work of Gadzuk.[54,55] Generalization of the model to current-driven dynamics is found in the work of Alavi et al.[56–58] Within this approach, the electron scattering event is described in the nuclear subspace by a series of instantaneous transitions between the ground and excited electronic states. The initial wave function is projected onto the resonance state, corresponding to a charge attachment to the fullerene, and the nuclei are allowed to evolve for a residence time τ_R before being instantaneously projected back to the neutral ground state, corresponding with electronic relaxation. To account for the continuous nature of the relaxation, this procedure is repeated for a range of resonance state residence times, and the observables are averaged over τ_R with an exponential weight function, $e^{-\tau_R/\tau}$, where τ is the resonance lifetime.

For the Au–C_{60}–Au system, previous calculations have found a resonance lifetime of 71.5 fs,[31] and this value is used also in the simulations of the Au–$Li@C_{60}$–Au system above. The initial wave function for the system is taken to be the ground vibrational state and is calculated on a coordinate grid subject

TABLE 2. Parameters for Calculating the Ground State Wavefunction and Nuclear Dynamics for Current-Driven Dynamics in the Au−Li@C_{60}−Au Junction[a]

parameter	value
Z_{max}	1.59 Å
Z_{min}	−1.59 Å
X_{max}	2.65 Å
X_{min}	−2.65 Å
nX	256
nZ	512
dt	1.0 fs
$d\tau_R$	1.0 fs

[a] The coordinate range used is indicated as well as the number of points per degree of freedom, time step (dt), and the residence time step $d\tau_R$.

to the potential of eq 1. The momentum operator incorporated in diagonalization of the Hamiltonian of the system is written within the Discrete Variable Representation (DVR),[59] and the nuclear dynamics are propagated using the split-operator technique.[60] The spatial and temporal parameters used in these calculations are collected in Table 2.

Acknowledgment. The authors acknowledge generous support from the W. M. Keck Foundation.

REFERENCES AND NOTES

1. Shinohara, H. Endohedral Metallofullerenes. *Rep. Prog. Phys.* **2000**, *63*, 843–892.
2. Vougioukalakis, G.; Roubelakis, M.; Orfanopoulos, M. Open-Cage Fullerenes: Towards the Constructrion of Nanosized Molecular Containers. *Chem. Soc. Rev.* **2010**, *39*, 817–844.
3. Chaur, M.; Melin, F.; Oritz, A.; Echegoyen, L. Chemical, Electrochemical, and Structural Properties of Endohedral Metallofullerenes. *Angew. Chem., Int. Ed.* **2009**, *48*, 7514–7538.
4. Dunsch, L.; Yang, S. Endohedral Clusterfullerenes—Playing with Cluster and Cage Sizes. *Phys. Chem. Chem. Phys.* **2007**, *9*, 3067–3081.
5. Saunders, M.; Cross, R.; Jimenez-Vazquez, H.; Shimshi, R.; Khong, A. Noble Gas Atoms Inside Fullerenes. *Science* **1996**, *271*, 1693–1697.
6. DiCammillo, B.; Hettich, R.; Guiochon, G.; Compton, R.; Saunders, M.; Jimenez-Vazquez, H.; Khong, A.; Cross, R. Enrichment and Characterization of a Noble Gas Fullerene: Ar@C_{60}. *J. Phys. Chem.* **1996**, *100*, 9197–9201.
7. Komatsu, K.; Murata, M.; Murata, Y. Encapsulation of Molecular Hydrogen in Fullerene C_{60} by Organic Synthesis. *Science* **2005**, *307*, 238–240.
8. Stevenson, S.; Rice, G.; Glass, T.; Harich, K.; Cromer, F.; Jordan, M.; Craft, J.; Hadju, E.; Bible, R.; Olmstead, M.; et al. Small-Bandgap Endohedral Metallofullerenes in High Yield and Purity. *Nature* **1999**, *401*, 55–57.
9. Murata, M.; Murata, Y.; Komatsu, K. Surgery of Fullerenes. *Chem. Commun.* **2008**, *46*, 6083–6094.
10. Cagle, D.; Kennel, S.; Saed, M.; Alford, J.; Wilson, L. *In Vivo* Studies of Fullerene-Based Materials using Metallofullerene Radiotracers. *Proc. Natl. Acad. Sci. U.S.A.* **1999**, *96*, 5182–5187.
11. Thrash, T.; Cagle, D.; Alford, J.; Wright, K.; Ehrhardt, G.; Mirzadeh, S.; Wilson, L. Toward Fullerene-Based Radiopharmaceuticals: High-Yield Neutron Activation of Endohedral 165Ho Metallofullerenes. *Chem. Phys. Lett.* **1999**, *308*, 329–336.
12. Kato, H.; Kanazawa, Y.; Okumura, M.; Taninaka, A.; Yokawa, T.; Shinohara, H. Lanthanoid Endohedral Metallofullerenols for MRI Contrast Agents. *J. Am. Chem. Soc.* **2003**, *125*, 4391–4397.
13. Bolskar, R.; Benedetto, A.; Husebo, L.; Price, R.; Jackson, E.; Wallace, S.; Wilson, L.; Alford, J. First Soluble M@C_{60} Derivatives Provide Enhanced Access to Metallofullerenes and Permit *In Vivo* Evaluation of Gd@C_{60}[C(COOH)$_2$]$_{10}$ as a MRI Contrast Agent. *J. Am. Chem. Soc.* **2003**, *125*, 5471–5478.
14. Harneit, W. Fullerene-Based Electron-Spin Quantum Computer. *Phys. Rev. A* **2002**, *65*, 32322.
15. Strózecka, A.; Muthukumar, K.; Dybek, A.; Dennis, J.; Larsson, J.; Myslivecek, J.; Voigtländer, B. Modification of the Conductance of Single Fullerene Molecules by Endohedral Doping. *App. Phys. Lett.* **2009**, *95*, 133118.
16. Zhao, J.; Feng, M.; Yang, J.; Petek, H. The Superatom States of Fullerenes and Their Hybridization into the Nearly Free Electron Bands of Fullerites. *ACS Nano* **2009**, *3*, 853–864.
17. Joachim, C.; Gimzewski, J.; Schlitter, R.; Chavy, C. Electronic Transparence of a Single C_{60} Molecule. *Phys. Rev. Lett.* **1995**, *74*, 2102–2105.
18. Park, H.; Park, J.; Lim, A.; Anderson, E.; Alivisatos, A.; McEuen, P. Nanomechanical Oscillations in a Single-C_{60} Transistor. *Nature* **2000**, *407*, 57–60.
19. Grobis, M.; Khoo, K.; Lu, X.; Nagaoka, K.; Louie, S.; Crommie, M.; Kato, H.; Shinohara, H. Spatially Dependent Inelastic Tunneling in a Single Metallofullerene. *Phys. Rev. Lett.* **2005**, *94*, 136802.
20. Taninaka, A.; Shino, K.; Sugai, T.; Heike, S.; Terada, Y.; Hashizume, T.; Shinohara, H. Scanning Tunneling Microscopy/Spectroscopy Studies of Lanthanum Endohedral Metallofullerenes. *Nano Lett.* **2003**, *3*, 337–341.
21. Jiang, J.; Gao, B.; Hu, Z.; Lu, W.; Wu, Z.; Yang, J.; Luo, Y. Identification of Metal-Cage Coupling in a Single Metallofullerene by Inelastic Electron Tunneling Spectroscopy. *Appl. Phys. Lett.* **2010**, *96*, 253110.
22. Wang, K.; Zhao, J.; Yang, S.; Chen, L.; Li, Q.; Wang, B.; Yang, S.; Yang, J.; Hou, J. G.; Zhu, Q. Unveiling Metal-Cage Hybrid States in a Single Endohedral Metallofullerene. *Phys. Rev. Lett.* **2003**, *91*, 185504.
23. Kobayashi, S.; Mori, S.; Iida, S.; Ando, H.; Takenobu, T.; Taguchi, Y.; Fujiwara, A.; Taninaka, A.; Shinohara, H.; Iwasa, Y. Conductivity and Field Effect Transistor of La_2@C_{80} Metallofullerene. *J. Am. Chem. Soc.* **2003**, *125*, 8116–8117.
24. Popok, V.; Azarko, I.; Gromov, A.; Jönsson, M.; Lassesson, A.; Campbell, E. Conductance and EPR Study of the Endohedral Fullerene Li@C_{60}. *Solid State Commun.* **2005**, *133*, 499–503.
25. Feng, M.; Zhao, J.; Petek, H. Atomlike, Hollow-Core-Bound Molecular Orbitals of C_{60}. *Science* **2008**, *320*, 359–362.
26. Huang, T.; Zhao, J.; Feng, M.; Petek, H.; Yang, S.; Dunsch, L. Superatom Orbitals of Sc_3N@C_{60} and Their Intermolecular Hybridization on the Cu(110)-(2 × 1)-O. *Phys. Rev. B* **2010**, *81*, 085434.
27. Feng, M.; Zhao, J.; Huang, T.; Zhu, X.-Y.; Petek, H. The Electronic Properties of Superatom States of Hollow Molecules. *Acc. Chem. Res.* **2011**, *44*, 360–368.
28. Kaun, C.; Seideman, T. Current-Driven Oscillation and Time-Dependent Transport in Nanojunctions. *Phys. Rev. Lett.* **2005**, *94*, 226801.
29. Jorn, R.; Seideman, T. Implications and Applications of Current-Induced Dynamics in Molecular Junctions. *Acc. Chem. Res.* **2010**, *43*, 1186–1194.
30. Seideman, T. Current-Driven Dynamics in Molecular-Scale Devices. *J. Phys.: Condens. Matter* **2003**, *15*, R521–R549.
31. Kaun, C.-C.; Jorn, R.; Seideman, T. Spontaneous Oscillation of Current in Fullerene Molecular Junctions. *Phys. Rev. B* **2006**, *74*, 045415.
32. Seideman, T. *Current-Driven Phenomena in Molecular-Scale Electronics*; Pan Stanford Publishing Pte. Ltd.: Singapore, 2010.
33. Jorn, R.; Seideman, T. Competition Between Current-induced Excitation and Bath-induced Decoherence in Molecular Junctions. *J. Chem. Phys.* **2009**, *131*, 244114.
34. Campbell, E.; Fanti, M.; Hertel, I.; Mitzner, R.; Zerbetto, F. The Hyperpolarisability of an Endohedral Fullerene: Li@C_{60}. *Chem. Phys. Lett.* **1998**, *288*, 131–137.
35. Aree, T.; Kerdcharoen, T.; Hannongbua, S. Charge Transfer, Polarizability and Stability of Li−C_{60} Complexes. *Chem. Phys. Lett.* **1998**, *285*, 221–225.
36. Zhang, M.; Harding, L.; Gray, S.; Rice, S. Quantum States of the Endohedral Fullerene Li@C_{60}. *J. Phys. Chem. A* **2008**, *112*, 5478–5485.

37. Tománek, D.; Li, Y. Ionicity of the M−C_{60} Bond in M@C_{60} Endohedral Complexes. *Chem. Phys. Lett.* **1995**, *243*, 42–44.
38. Slanina, Z.; Uhlík, F.; Lee, S.-L.; Adamowicz, L.; Nagase, S. MPWB1K Calculations of Stepwise Encapsulations: Li*x*@C_{60}. *Chem. Phys. Lett.* **2008**, *463*, 121–123.
39. Pavanello, M.; Jalbout, A.; Trzaskowski, B.; Adamowicz, L. Fullerene as an Electron Buffer: Charge Transfer in Li@C_{60}. *Chem. Phys. Lett.* **2007**, *442*, 339–343.
40. Li, Y.; Tománek, D. How Free are Encapsulated Atoms in C_{60}. *Chem. Phys. Lett.* **1994**, *221*, 453–458.
41. Broclawik, E.; Eilmes, A. Density Functional Study of Endohedral Complexes M@C_{60} (M = Li, Na, K, Be, Mg, Ca, La, B, Al): Electronic Properties, Ionization Potentials, and Electron Affinities. *J. Chem. Phys.* **1998**, *108*, 3498–3503.
42. Dunlap, B.; Ballester, J.; Schmidt, P. Interactions Between C_{60} and Endohedral Alkali Atoms. *J. Phys. Chem.* **1992**, *96*, 9781–9787.
43. Gromov, A.; Krawez, N.; Lassesson, A.; Ostrovskii, D.; Campbell, E. Optical Properties of Endohedral Li@C_{60}. *Curr. Appl. Phys.* **2002**, *2*, 51–55.
44. Hernández-Rojas, J.; Bretón, J.; Gomez Llorente, J. Rotational Spectra for Off-Center Endohedral Atoms at C_{60} Fullerene. *J. Chem. Phys.* **1996**, *104*, 1179–1186.
45. Joslin, C.; Gray, C.; Goldman, S.; Yang, J.; Poll, J. Raman Spectra of Endohedral Fullerenes. Li + C_{60}. *Chem. Phys. Lett.* **1993**, *215*, 144–150.
46. Joslin, C.; Yang, J.; Gray, C.; Goldman, S.; Poll, J. Infrared Rotation and Vibration-Rotation Bands of Endohedral Fullerene Complexes. K + C_{60}. *Chem. Phys. Lett.* **1993**, *211*, 587–594.
47. Butz, T. *Fourier Transformation for Pedestrians*; Springer: New York, 2006.
48. Vrakking, M.; Villeneuve, D.; Stolow, A. Observation of Fractional Revivals of a Molecular Wave Packet. *Phys. Rev. A* **1996**, *54*, R37–R40.
49. Sainoo, Y. Excitation of Molecular Vibrational Modes with Inelastic Scanning Tunneling Microscopy Processes: Examination Through Action Spectra of *cis*-2-butene on Pd(110). *Phys. Rev. Lett.* **2005**, *95*, 246102.
50. Petek, H.; Weida, M.; Nagano, H.; Ogawa, S. Real-Time Observation of Adsorbate Atom Motion Above a Metal Surface. *Science* **2000**, *288*, 1402–1404.
51. Ishioka, K.; Hase, M.; Kitajima, M.; Wirtz, L.; Rubio, A.; Petek, H. Ultrafast Electron-Phonon Decoupling in Graphite. *Phys. Rev. B* **2008**, *77*, 121402.
52. Menzel, D.; Gomer, R. Desorption from Metal Surfaces by Low-Energy Electrons. *J. Chem. Phys.* **1964**, *41*, 3311.
53. Redhead, P. Interaction with Slow Electrons with Chemisorbed Oxygen. *Can. J. Phys.* **1964**, *42*, 886.
54. Gadzuk, J. The Semiclassical Way to Molecular-Dynamics at Surfaces. *Annu. Rev. Phys. Chem.* **1988**, *39*, 395–424.
55. Gadzuk, J. Resonance-Assisted, Hot-Electron-Induced Desorption. *Surf. Sci.* **1995**, *342*, 345–358.
56. Alavi, S.; Rousseau, R.; Seideman, T. Toward Control of Surface Reactions with a Scanning Tunneling Microscope. Structure and Dynamics of Benzene Desorption from a Silicon Surface. *J. Chem. Phys.* **2000**, *113*, 4412–4423.
57. Alavi, S.; Rousseau, R.; Patitsas, S.; Lopinski, G.; Wolkow, R.; Seideman, T. Inducing Desorption of Organic Molecules with a Scanning Tunneling Microscope: Theory and Experiments. *Phys. Rev. Lett.* **2000**, *85*, 5372–5375.
58. Alavi, S.; Rousseau, R.; Lopinski, G.; Wolkow, R.; Seideman, T. Controlling Organic Reactions on Silicon Surfaces with a Scanning Tunneling Microscope: Theoretical and Experimental Studies of Resonance-Mediated Desorption. *Faraday Discuss.* **2000**, *117*, 213–229.
59. Colbert, D.; Miller, W. A Novel Discrete Variable Representation for Quantum-Mechanical Reactive Scattering *via* the S-Matrix Kohn Method. *J. Chem. Phys.* **1992**, *96*, 1982–1991.
60. Fleck, J.; Morris, J.; Feit, M. Time-Dependent Propagation of High-Energy Laser-Beams Through Atmosphere. *Appl. Phys.* **1976**, *10*, 129–160.